



Improving the Morphological and Optical Properties of Sputtered Indium Tin Oxide Thin Films by Adopting Ultralow-Pressure Sputtering

Myung Soo Huh,^{a,b} Bong Seop Yang,^a Jaewon Song,^a Jaeyeong Heo,^a Seok-Jun Won,^a Jae Kyeong Jeong,^c Cheol Seong Hwang,^{a,*} and Hyeong Joon Kim^{a,z}

^aDepartment of Materials Science and Engineering and Inter-University Semiconductor Research Center, Seoul National University, Seoul 151-744, Korea

^bSamsung SDI Company, Limited, Core Technology Laboratory, Gyeonggi-Do 442-391, Korea

^cSamsung SDI Company, Limited, Corporate Research and Development Center, Gyeonggi-Do 449-902, Korea

The morphological and optical properties of indium tin oxide (ITO) thin films deposited by an ultralow-pressure dc magnetron sputtering (ULPS) method followed by postannealing treatment at 250°C are reported. The surface roughness of the film (R_{rms} : 0.5 nm) deposited using ULPS was about 5 times lower than that of the film (R_{rms} : 2.7 nm) sputtered using a pressure of 6.7×10^{-1} Pa. ITO thin films with a low resistivity of $3.7 \times 10^{-4} \Omega \text{ cm}$ were also achieved using a continuous two-step deposition process, in which the initial layer was deposited using ULPS and then the final layer was deposited with a SP of 6.7×10^{-1} Pa, without the use of any other additional steps. Both the ULPS and continuous two-step deposition methods were found to be effective for producing ITO thin films with enhanced morphologies that make them suitable for use in display devices.

© 2008 The Electrochemical Society. [DOI: 10.1149/1.3005562] All rights reserved.

Manuscript submitted June 26, 2008; revised manuscript received September 3, 2008. Published November 5, 2008.

Indium tin oxide (ITO) thin films are highly degenerate, wide-bandgap semiconductors (E_g : 3.4–4.3 eV). They have a low electrical resistivity due to their high carrier concentration, and the location of their Fermi level is above the lower edge of the conduction band.^{1–3} ITO films also exhibit a high level of transmission in the visible near-infrared regions of the electromagnetic spectrum. Due to these unique properties, ITO thin films have been widely studied for their potential use in the optoelectronics industry and display devices, such as solar-control windshield glass, solar cells, organic light-emitting displays (OLEDs), flexible display devices, and transparent, flexible electronic circuit boards.^{3–5} Smooth surface morphology with high electrical conductivity is the crucial factor for the current driven devices such as OLEDs. So far, several methods have been employed to prepare ITO thin films. Examples include spray pyrolysis, reactive evaporation, pulsed laser deposition, conventional magnetron sputtering, cesium-ion-induced magnetron sputtering, and ion-beam assisted sputtering.^{6–11} Among these deposition methods, magnetron sputtering is preferable, because it allows easy process control for the device structure and the production of display devices with large areas. However, one of the practical drawbacks of using sputtered ITO thin films for display device applications is their rough surface morphology. This makes them unsuitable for use as the semiconducting layer or transparent electrode of display devices. For example, the quality of the interface between the ITO electrode and the organic emitting layer is crucial to the performance of OLEDs.^{12–15} Using a rough ITO layer as the anode may cause undesired electrical shorts or decrease the contact area between the emitting layers and the anode and even form bubbles to deteriorate the color quality and lifetime of the emitting area.^{12,16} These functional properties of ITO thin films are strongly dependent on their microstructures, which are influenced by the deposition method and processing conditions used to make them.

In this study, ITO thin films with smooth surface morphologies were obtained using an ultralow-pressure dc magnetron sputtering (ULPS) method. A ULPS method means that the sputtering pressure (SP) is below 1.3×10^{-1} Pa. It was found that the SP largely affects the surface morphology and crystalline structures of the films. By comparing the films deposited by ULPS with those obtained by the conventional sputtering method (which uses a pressure of 6.7×10^{-1} Pa), it was shown that the surface roughness of the former was 5 times lower. The ULPS method also resulted in films with high transparency in the visible range. However, their electrical properties were not suitable for transparent electrode applications. In order to obtain films with low resistivities and smooth surface morphologies, we used a continuous two-step deposition method. We achieved low-resistivity ITO thin films ($3.7 \times 10^{-4} \Omega \text{ cm}$) using this two-step method, in which the initial and final layers were deposited using pressures of 6.7×10^{-2} and 6.7×10^{-1} Pa, respectively. No other steps were required. ULPS was found to be effective for producing ITO thin films with enhanced surface morphologies that make them suitable for use in display devices.

× 10⁻¹ Pa), it was shown that the surface roughness of the former was 5 times lower. The ULPS method also resulted in films with high transparency in the visible range. However, their electrical properties were not suitable for transparent electrode applications. In order to obtain films with low resistivities and smooth surface morphologies, we used a continuous two-step deposition method. We achieved low-resistivity ITO thin films ($3.7 \times 10^{-4} \Omega \text{ cm}$) using this two-step method, in which the initial and final layers were deposited using pressures of 6.7×10^{-2} and 6.7×10^{-1} Pa, respectively. No other steps were required. ULPS was found to be effective for producing ITO thin films with enhanced surface morphologies that make them suitable for use in display devices.

Experimental

The ITO thin films were deposited by dc magnetron sputtering using a five-angle cluster-type system (CSP5000, SNtek Corp.). This was performed on a stationary substrate by a deposition-down method in the sputtering module at room temperature. To obtain ULPS (< 1.3×10^{-1} Pa), the magnetic housing of the cathode was designed to maximize the magnetic field on the surface of the target and to minimize the distance between the center and edge magnets. An In_2O_3 target (purity: 99.99%) that contained 10 wt % SnO_2 was used. Corning 1737 glass and a Si wafer were used as the substrates. The distance between the substrate and the target was about 10 cm. Argon was used as the sputtering gas at a constant dc power of 2.2 W/cm². The base pressure before deposition was below 6.7×10^{-5} Pa, and the SP was either 6.7×10^{-1} or 6.7×10^{-2} Pa. Following the ITO deposition, the films were vacuum annealed at 250°C for 30 min. With the aim of obtaining higher-quality ITO thin films, we also investigated the use of a continuous two-step deposition method. This involved depositing initial and final layers using pressures of 6.7×10^{-1} and 6.7×10^{-2} Pa, respectively.

The thickness of each deposited ITO thin film was approximately 200 nm, as measured by surface profilometry (Nanospec AFT/200, KLA-Tencor) and cross-sectional field-emission scanning electron microscopy (FE-SEM, S-4800, Hitachi). The surface morphologies and cross-sectional structures of the ITO films were investigated by atomic force microscopy (AFM, XE-150, PSIA) and FE-SEM. The optical transmittance properties of the films were measured using a UV-visible single-beam spectrometer (Lambda 45, Perkin-Elmer). Standard Θ-2Θ X-ray diffraction (XRD) measurements were performed using Cu Kα radiation at 40 kV and 30 mA (X'pert pro, PANalytical). The compositions and chemical properties of the films

* Electrochemical Society Active Member.
 z E-mail: thinfilm@snu.ac.kr

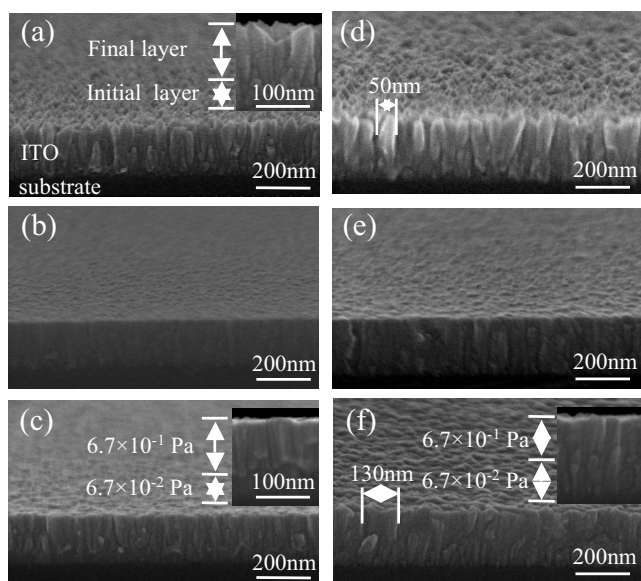


Figure 1. Cross-sectional SEM images of the ITO thin films produced under SPs of 6.7×10^{-1} and 6.7×10^{-2} Pa and by the continuous SF; (a)–(c) as-deposited ITO thin films and (d)–(f) after postannealed films. (a) and (d) SP: 6.7×10^{-1} Pa, (b) and (e) SP: 6.7×10^{-2} Pa, and (c) and (f) TSF.

were analyzed using X-ray photoelectron spectroscopy (XPS, Sigma Probe, Thermo VG). The electrical resistivity, free carrier concentration, and Hall mobility were determined from Hall-effect measurements, employing the van der Pauw geometry (HL5500PC, BIO-RAD). The magnetic field was fixed at 0.5 T.

Results and Discussion

Figures 1a–c show the cross-sectional SEM images of the as-deposited ITO thin films produced using SPs of 6.7×10^{-1} and 6.7×10^{-2} Pa and those fabricated by the continuous two-step deposition method. As the SP was decreased from 6.7×10^{-1} to 6.7×10^{-2} Pa, the structure of the resulting film transformed from a columnar structure to a dense fibrous one, and the surface morphology of the film changed from rough to smooth. As shown in Fig. 1a, the as-deposited ITO thin film produced using a pressure of 6.7×10^{-1} Pa appears to be composed of two layers, viz. an amorphous (or nanosized) structure adjacent to the substrate and a rough-surfaced polycrystalline structure on top. These results are similar to those in reports by Vink et al., Meerakker et al., and Hoheisel et al., who found that the double-layer structures of as-deposited ITO thin films fabricated using a SP of 5.0×10^{-1} Pa consisted of amorphous (or nanosized) and polycrystalline layers.^{17–20} In general film growth, the initial layers grow on top of the substrate, and later thicker layers grow on the growing films themselves, which usually induce a non-negligible change in microstructure during the film growth. This seems to be somehow more evident in this ITO sputtering case. In addition, there appears to be another factor that influences the microstructure, as mentioned below.

The studies of Hoheisel et al. and Neerinck et al. have reported that the sputtering rate slightly decreases while the film is depositing.^{19,20} The oxygen flow rate is constant during a sputtering process. The balance between the amount of sputtered particles and oxygen depends on the sputtering rate, which slightly shifts into the oxygen-rich condition as the deposition time increases. Therefore, the initial layer of ITO thin films in Fig. 1a is deposited at a higher rate than the final layer because of the relatively lower oxygen concentration during the initial growth stage. Therefore, the initial layer may have poorer crystalline quality with smaller grain size or even an amorphous structure. Then, with the decrease in sputtering rate at the later stage of the sputtering process, oxygen-rich grains emerge

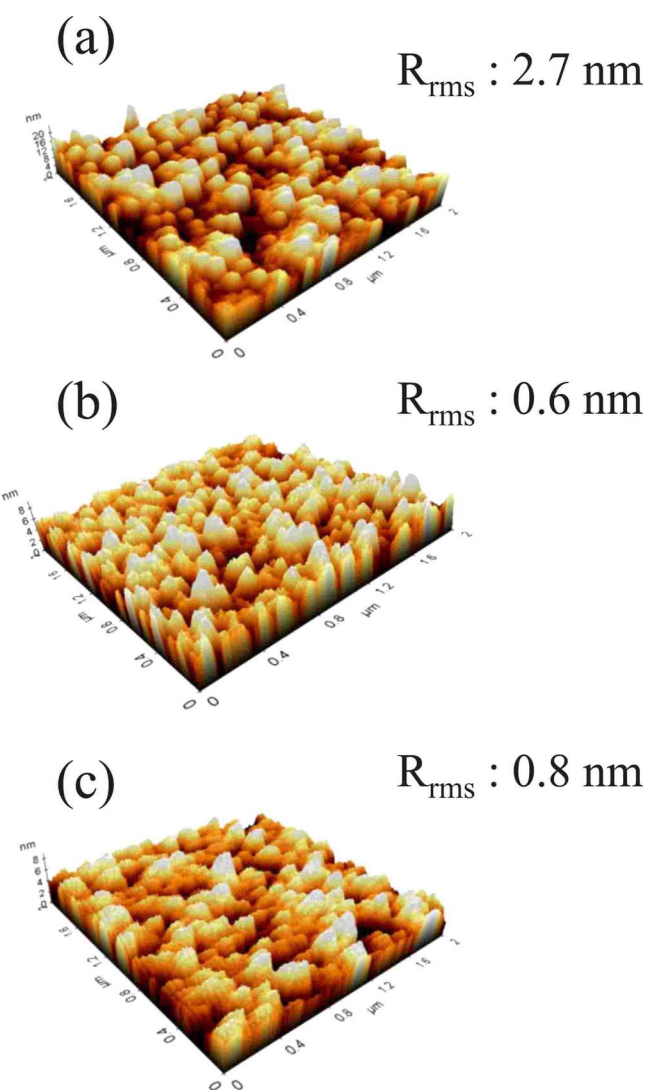


Figure 2. (Color online) AFM images ($2 \times 2 \mu\text{m}$) of the postannealed ITO films produced under SPs of 6.7×10^{-1} and 6.7×10^{-2} Pa and by the continuous TSF: (a) 6.7×10^{-2} Pa, (b) 6.7×10^{-1} Pa, and (c) TSF.

in its upper part. To conclude, as shown in Fig. 1a, the sputtered ITO thin films appeared to be composed of two layers, an amorphous (or nanosized) structure adjacent to the substrate and a polycrystalline structure on top with a rough surface. However, the low-pressure sputtered ITO film (made by ULPS, Fig. 1b) appears to be composed of only a single layer with an extremely smooth surface. We suppose that the low-pressure sputtered film has a dense structure with narrow columns because the increasing energy of the sputtered particles with decreasing SP hinders the growth of the columnar structures. The scattering effect of the sputtered particles is larger for the conventional SP (6.7×10^{-1} Pa) than for the ULPS (6.7×10^{-2} Pa), because the sputtered particles frequently undergo collisions with the sputter gas during their migration to the substrate, thereby developing an oblique component.^{21,22} That is, the sputtered particles in the low-SP approach in a direction near-normal to the substrate. The oblique components are higher for the conventional SP than for the ULPS and are closely related to the formation of columnar structure. These results suggest that the surface morphologies of the ITO films are strongly dependent on the SP. The cross-sectional SEM images in Fig. 1d–f exhibit the surface roughness and columnar structure of the films after they were postannealed at 250°C for 30 min. After postannealing, columnar structures are clearly observed in all cases. The AFM images in Fig. 2 show the

Table I. Properties of the ITO thin films deposited at various SPs with a dc power of 2.2 W/cm² and the continuous TSFs, after being vacuum annealed at 250°C for 30 min.

	6.7×10^{-1} Pa	1.3×10^{-1} Pa	6.7×10^{-2} Pa	TSF
Average surface roughness (nm)	2.7	0.9	0.6	0.8
Resistivity (Ω cm)	1.2×10^{-3}	7.2×10^{-3}	1.1×10^{-2}	3.7×10^{-4}
Mobility (cm ² /V s)	1.42	1.73	8.69	8.47
Carrier concentration (cm ⁻³)	3.6×10^{21}	5.0×10^{20}	6.8×10^{19}	2.0×10^{21}
Transmittance (550 nm)	>80%	>85%	>85%	>80%

surface morphologies of the postannealed ITO films deposited using SPs of 6.7×10^{-1} and 6.7×10^{-2} Pa and that of the film grown by the continuous two-step deposition method. Table I summarizes the average surface roughness (R_{rms}) data of these films (and those of the films prior to postannealing), including the electrical and optical results. As shown in Fig. 2 and Table I, upon postannealing, the R_{rms} values of the ITO films deposited using pressures of 6.7×10^{-1} and 6.7×10^{-2} Pa increase from 1.6 to 2.7 nm and from 0.4 to 0.6 nm, respectively. On the basis of the above results, we can confirm that we have obtained ITO films that have lower surface-roughness values (R_{rms} ; 0.6 nm) than those previously reported (R_{rms} ; <3.2 nm).^{4,10,16} No additional processing steps, such as the addition of H₂O, chemical mechanical polishing, or ion-beam treatment, were used in our methods. According to the electrical data (resistivity and carrier density) in Table I, decreasing the SP is also found to affect the electrical properties of the ITO thin films. It is found that the resistivity of the films increases from 1.2×10^{-3} to 1.1×10^{-2} Ω cm for SP from 6.7×10^{-1} to 6.7×10^{-2} Pa. This increase in resistivity with a decrease in SP can be explained by the number of oxygen vacancies in the ITO thin film. The oxygen vacancies create free electrons in the film because one oxygen vacancy generates two extra electrons. An increase in the number of oxygen vacancies leads to an increase in carrier concentration. As the SP decreases from 6.7×10^{-1} to 6.7×10^{-2} Pa, the carrier concentration decreases from 3.6×10^{21} to 6.8×10^{19} cm⁻³. This decrease can be explained by the increase in the effective oxygen-gas concentration in the sputter gas. This is because the only source of oxygen atoms (or ions) during the sputtering is the ITO target; no oxygen gas was added to the sputter gas. The decrease in SP is performed by reducing the Ar-gas flow rate, which results in an increase in the effective oxygen concentration in the sputter gas. It is estimated that the oxygen gas ratio at 6.7×10^{-2} Pa is about 1 order of magnitude higher than that at 6.7×10^{-1} Pa. Next, we study the continuous two-step deposited films (TSFs), in which the initial and final layers were produced using pressures of 6.7×10^{-2} and 6.7×10^{-1} Pa, respectively. As shown in Fig. 1c and f, the diameters of columns of the continuous TSF are larger than those of the as-deposited and postannealed films made using a pressure of 6.7×10^{-1} Pa (see Fig. 1a and d). It is estimated that the initial layer (deposited by ULPS), which consisted of a dense fibrous structure, hinders the growth of the amorphous (or nanosized) layer during the deposition at 6.7×10^{-1} Pa. Therefore, the final layer (deposited at 6.7×10^{-1} Pa) has a larger columnar structure. Following the postannealing treatment of those films, the rate of increase in surface roughness of the continuous TSF is about two times lower than that of the postannealed film deposited at 6.7×10^{-1} Pa (see Fig. 2a and c). To be exact, upon the postannealing treatment, the surface roughness of the former film increases from 0.6 to 0.8 nm and that of the latter from 1.6 to 2.7 nm. The lower rate of increase in surface roughness of the postannealed TSF is thought to originate from the smooth surface morphology of the initial underlying layer deposited using ULPS. The lower surface roughness corresponds to the lower specific surface area (surface area for the given volume) compared to the rougher surface. Therefore, the driving force for the grain growth (increase in roughness) should be lower for the smoother surface.

The XRD patterns of the 200 nm thick ITO films deposited using SPs of 6.7×10^{-1} and 6.7×10^{-2} Pa and by the continuous two-step deposition method are shown in Fig. 3. The as-deposited film (see Fig. 3c) produced at the conventional SP of 6.7×10^{-1} Pa has a nanocrystalline structure with diffraction peaks corresponding to the (211), (222), (400), (440), and (622) reflections of the In₂O₃ crystal. The low-pressure deposited ITO thin film (made via ULPS) mainly shows the (222) peak, but a weak (400) peak is also observed. The (400) diffraction peak of the In₂O₃ crystal is observed as a shoulder of the broad amorphous In₂O₃ peak. This shoulder peak becomes more intense as the SP is increased from 6.7×10^{-2} to 6.7×10^{-1} Pa. The lower intensity of the (400) diffraction peak for the low-pressure deposited film is thought to be caused by the following two factors: (i) the enhanced energy of the sputtered particles due to the minimization in the scattering effect and (ii) the increase in the effective oxygen-gas concentration in the sputter gas. First, we consider the influence of decreasing the SP on the energy of the sputtered particles. The energy loss of a sputtered particle as it passes through the Ar sputtering gas can be estimated from the following (Kevin Meyer) equation²³

$$E_F = (E_0 - k_B T_G) \exp \left[n \ln \left(\frac{E_F}{E_i} \right) \right] + k_B T_G \quad [1]$$

where E_F is the energy of the sputtered particle as it arrives at the substrate, E_0 is the energy of the sputtered particle as it leaves the target, T_G is the sputtering gas temperature, E_f/E_i is the ratio of energies before and after a collision, and n is the number of collisions that take place in the gas. Here, n and E_f/E_i are given by

$$n = \frac{dP_w \sigma}{k_B T_G} \quad [2]$$

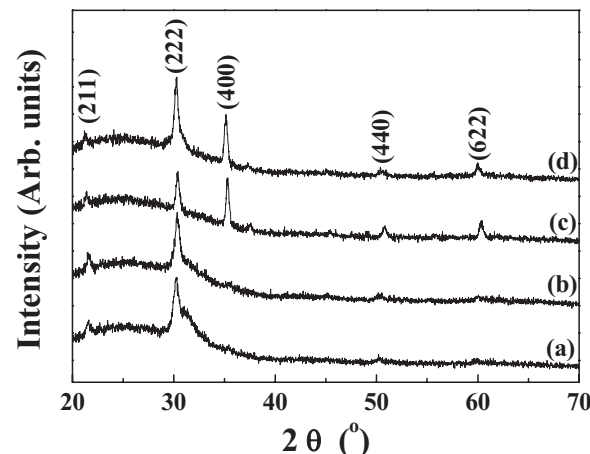


Figure 3. XRD patterns of the ITO thin films produced by dc magnetron sputtering using Ar gas as the sputter gas under various SPs and by the continuous TSF: (a) 6.7×10^{-2} Pa, (b) 1.3×10^{-1} Pa, (c) 6.7×10^{-1} Pa, and (d) TSF.

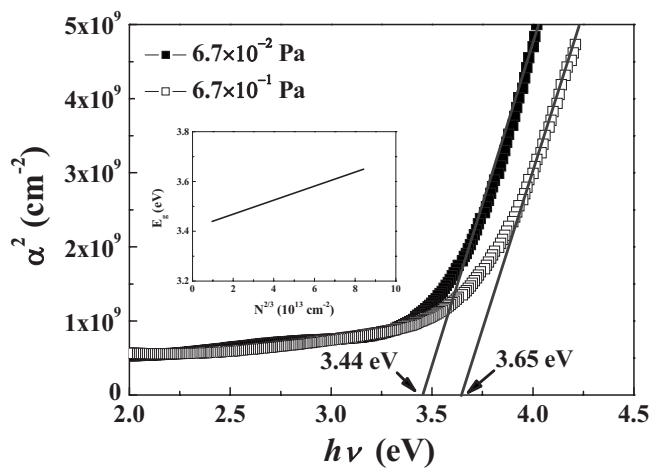


Figure 4. Optical bandgap energies of the ITO films produced under a SP of either 6.7×10^{-1} (-□-) or 6.7×10^{-2} Pa (-■-). The inset shows the intrinsic bandgap as a function of $N^{2/3}$ for the ITO films under the same conditions.

$$\frac{E_f}{E_i} = 1 - \frac{2\eta}{(1 + \eta)^2} \quad [3]$$

where d is the distance traveled, P_w is the SP, σ is the collision cross section (assuming hard core interactions), and η is the atomic mass ratio of the colliding particles.²⁴ Using the above equation, the E_f of the Ar arriving at the substrate surface is about 60% higher for the SP of 6.7×10^{-2} Pa than that for 6.7×10^{-1} Pa. This result is similar to the report by Winters et al., who described the relationship between the energy of sputtered particles and the SP. They determined that the energy of the sputtered particles was attenuated by gas-phase collisions, and so their incorporation into the growing film decreased with increasing SP.²⁵ Second, the XRD data was investigated as a function of SP. The integrated intensity ratio of the (400) diffraction peak to the (222) peak [$I(400)/I(222)$] is 0.36 for the films deposited using ULPS. By contrast, the value for the random orientation by the American Standards for Testing Materials is 0.33, which indicates a preferred orientation of the grains in the $\langle 111 \rangle$ direction. With decreasing the SP, the preference for the $\langle 111 \rangle$ direction became stronger. This exhibits the same tendency as the predominant orientation with increasing oxygen-gas ratio for the sputtered ITO films.^{5,26,27} It turns out that the effective oxygen-gas concentration in the sputter gas increases with decreasing the SP. As shown by the carrier-concentration values in Table I, decreasing the SP results in an increase in the effective oxygen-gas concentration in the sputter gas. Therefore, we suggest that the decrease in the preferred orientation along the (400) plane originated from the enhanced energy of the incident sputtered particles and the increased effective oxygen-gas concentration in the sputter gas due to the ULPS.

The effect of wavelength on the transmittance (T) of the ITO thin films is closely related to the absorption coefficient. The optical bandgap energies of the as-deposited ITO thin films (deposited using ULPS and the conventional SP of 6.7×10^{-1} Pa) are shown in Fig. 4. The absorption coefficients of the films at different wavelengths are calculated from the transmission and reflection data.²⁶ The following relationship was used to determine the energy bandgap from the absorption coefficient data²⁸

$$\alpha h\nu \approx (h\nu - E_g)^{1/2} \quad [4]$$

where α is the absorption coefficient, $h\nu$ is the photon energy, and E_g is the optical energy bandgap. Extrapolations of the straight regions of the plots to $\alpha = 0$ give E_g . As shown in Fig. 4, the absorption edge moves from about 3.65–3.44 eV when the SP decreases from 6.7×10^{-1} to 6.7×10^{-2} Pa. This shift is due to the decrease in the SP, as shown in Table I. This means that the decrease in the

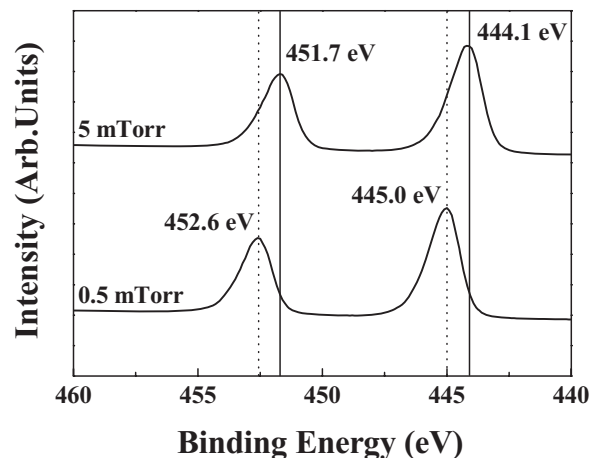


Figure 5. In 3d XPS spectra of the ITO thin films produced under a SP of (a) 6.7×10^{-1} Pa and (b) 6.7×10^{-2} Pa.

carrier concentration lowers the Fermi level. These values are similar to the results quoted in previous reports.^{1,26} As the SP increases, the absorption edge shifts toward a higher energy. The widening of the energy bandgap can be explained on the basis of the Burstein-Moss shift.²⁹ This shift of the energy can be written as follows

$$E_g - E_{go} = \frac{\pi^2 h^2}{2m_r^*} \left(\frac{3N}{\pi} \right)^{2/3} \quad [5]$$

where E_{go} is the intrinsic bandgap, h is Planck's constant, and m_r^* is the reduced effective mass. The shift of the bandgap with the change in the carrier concentration (N) is further elaborated in the inset of Fig. 4. The linearity of the curve shows that the widening of the bandgap is proportional to $N^{2/3}$. This effect, i.e., the widening of the bandgap with increasing N , is exhibited when the electron density far exceeds the Mott critical density, which is written as³⁰

$$N \gg \sqrt[3]{\frac{\pi^2 m_c^* e^2}{\epsilon_0 h^2}} \quad [6]$$

where e is the electron charge, ϵ_0 is the permittivity of free space, and m_c^* is the conduction-band effective mass. Under the condition that N greatly exceeds the Mott critical density, the conduction band is partly filled, i.e., its lowest states are blocked, which leads to the widening of the bandgap.^{30,31} The intrinsic absorption edge, found by the extrapolation of E_g to $N = 0$, is $E_{go} = 3.42$ eV, which is in good agreement with the value obtained by Swati Ray et al. (~ 3.52 eV).¹ As N decreases with decreasing the SP from 6.7×10^{-1} to 6.7×10^{-2} Pa, E_g decreases. This is in agreement with the variation indicated in Eq. 5. The decrease in N with increasing effective oxygen-gas concentration implies that the carriers originated from oxygen vacancies (see Table I).

Figure 5 shows In 3d XPS spectra of the ITO thin films deposited using the SPs of 6.7×10^{-2} or 6.7×10^{-1} Pa. It was found that the In 3d peaks of the films deposited by ULPS were clearly shifted to the higher binding energy side compared with the In 3d peaks of the films deposited at 6.7×10^{-1} Pa. When a metal combines with oxygen to become a compound, its inner-shell electron binding energy increases slightly.³² Therefore, we suggest that the shift of the In 3d binding energy of the films deposited by ULPS is caused by the increased formation of indium oxide phase in the films. The electronic-transport behavior of these films strongly depends on the number of oxygen vacancies that are generated and compensated.³³ The electronic conduction of semiconductor oxides is thought to be strongly dependent on their ionicity. We suggest that the high resis-

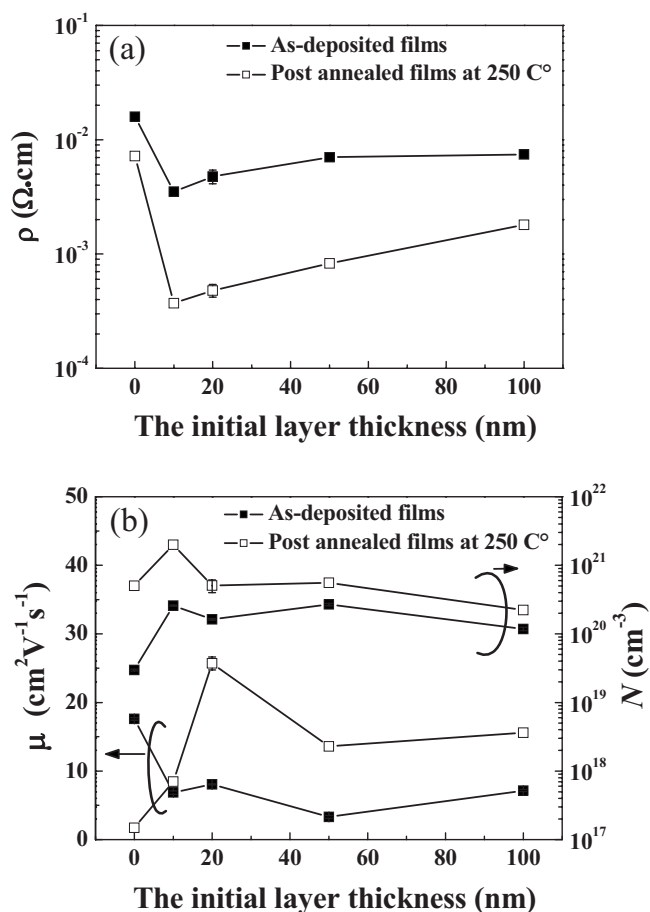


Figure 6. Dependence of the (a) electrical resistivity and (b) carrier concentration and Hall mobility of the continuous TSFs on the initial layer thickness: (-■-) as-deposited films and (-□-) postannealed films.

tivities of the ITO thin films deposited by ULPS have originated from their dense, fibrous structures that have low carrier concentrations.^{32,33}

We successfully fabricated ITO thin films with remarkably smooth surface morphologies using ULPS. Incidentally, as shown in Table I, their high resistivities make them unsuitable for transparent conductive oxide (TCO) applications. The resistivities of the low-pressure sputtered ITO films (using ULPS) are higher than those of the films sputtered at 6.7×10^{-1} Pa. In order to obtain films with low resistivities and smooth surface morphologies, we designed the continuous two-step deposition method. This method produces films that have a combination of the merits of the films deposited at 6.7×10^{-2} and 6.7×10^{-1} Pa. That is, they each exhibit an extremely smooth surface morphology (comparable to that of the films obtained by ULPS) and a low resistivity (comparable to that of the films deposited at 6.7×10^{-1} Pa).

The variation in electrical properties (resistivity, carrier density, and Hall mobility) as a function of the initial layer thickness is shown in Fig. 6. The resistivities (ρ) of the as-deposited films decrease from 1.6×10^{-2} to 3.5×10^{-3} $\Omega \cdot \text{cm}$ as the initial layer thickness is increased up to 10 nm, as shown in Fig. 6a. An increase in the initial layer thickness from 10 to 100 nm increases the ρ of the films from 3.5 to 7.4×10^{-3} $\Omega \cdot \text{cm}$. This is because the contribution of the final layer to the ρ of the films is diminished. Figure 6b shows the electron mobility (μ) and carrier concentration (N) of the films as a function of the thickness of the initial layer. As the thickness of the initial layer increases from 0 to 10 nm, N increases from about 3.0×10^{19} to 2.6×10^{20} cm^{-3} , while μ decreases from about 17.6 to $6.9 \text{ cm}^2/\text{V s}$. Following the postannealing at 250°C for 30 min, ρ decreases to about one-tenth of its original value. As shown in Fig. 1c and f, we estimate that the low resistivities of the continuous TSFs originate from the increase in the columnar size of the final layers. The columnar diameters in the final layer in the continuous TSF and those of the film deposited at 6.7×10^{-1} Pa are about 130 and 50 nm, respectively. Therefore, the columns are about 2.5 times wider in the films produced by the continuous two-step deposition method. As the columnar size increases, the ρ of the continuous TSFs is rapidly decreased. Most studies have reported that the electrical properties of ITO films are closely related to the surface roughness and columnar size, which are both influenced by postannealing conditions.^{29,34,35} For the above reasons, smooth ITO films with a minimum resistivity of about 3.7×10^{-4} $\Omega \cdot \text{cm}$ are achieved by the continuous two-step deposition method. This resis-

Table II. Comparison of TCO performance and other results.

Conditions (nm)	R_s (Ω/\square)	Transmittance at different wavelengths (nm)				Figure of merit ($\times 10^{-3} \Omega^{-1}$) at different wavelengths (nm)			
		400	500	600	700	400	500	600	700
Our films	TSF ^a (190/10)	18.6	0.78	0.78	0.89	0.92	4.5	4.5	16.7
	TSF ^a (180/20)	24.0	0.85	0.75	0.84	0.95	8.2	2.3	7.3
	TSF ^a (150/50)	41.4	0.84	0.78	0.86	0.98	4.2	2.0	5.3
	TSF ^a (100/100)	90.1	0.85	0.82	0.87	0.99	2.2	1.5	2.7
	ULPS (6.7×10^{-2} Pa)	702.0	0.61	0.89	0.99	0.93	—	0.4	1.3
Other films	CP ^b (6.7×10^{-1} Pa)	80.7	0.71	0.93	0.92	0.86	0.4	6.0	5.4
	Wang et al. ⁶	40.0	—	0.70	—	—	0.2	—	—
	Ishibashi et al. ³⁰	36.0	0.82	0.87	0.82	0.82	3.8	6.9	3.8

^a TSF (thickness of the initial layer/the thickness of final layer): the continuous TSFs.

^b CP: conventional sputtering method.

tivity value is lower than previously reported values, which were about $6.4 \times 10^{-4} \Omega \text{ cm}$ when using only Ar gas and a SP of $6.7 \times 10^{-1} \text{ Pa}$.^{33,36,37}

The evaluation of these transparent electrodes for practical applications, such as display devices, optical devices, and solar cells, is carried out by determining the relationship between the optical transmittance (T) and the sheet resistance (R_s). To evaluate the performance of transparent conducting films, Haake et al. defined the “figure of merit” (Φ_{TC}), which is the ratio of the transmittance to R_s .³⁸ It is given by

$$\Phi_{TC} = \frac{T^{10}}{R_s} \quad [7]$$

The figure-of-merit values for the continuous TSFs, as exhibited in Fig. 6, and the ITO thin films, as listed in Table I, are shown in Table II, along with some of the values obtained by other researchers.^{8,37} Table II shows that the figures of merit for the continuous TSFs are similar to those for the other films at a wavelength of 500 nm. However, the continuous TSFs had much smoother surfaces than the other films.

Conclusion

In this paper, the surface morphology and the optical and electrical properties of low-pressure sputtered ITO films (produced using ULPS) are reported and compared with those of ITO films sputtered at $6.7 \times 10^{-1} \text{ Pa}$. As the SP was decreased, the structure of the ITO films changed from a columnar structure to a dense, fibrous structure. In addition, the surface roughness was reduced from about 2.7 to 0.6 nm (R_{rms}). We believe these changes to be caused by the following two factors: (i) the increase in the effective oxygen concentration in the sputter gas and (ii) the increase in the E_f of the sputtered particles due to the decrease in the SP. The increase in the effective oxygen concentration in the sputter gas affected the integrated intensity ratio of the (222) diffraction peak to the (400) peak [$I(222)/I(400)$], shifted the optical bandgap energy from 3.65 to 3.44 eV, decreased N from 3.6×10^{21} to $6.8 \times 10^{19} \text{ cm}^{-3}$, and increased the resistivity of the films. We showed that the SP was closely related to the structural, electrical, and optical properties of the ITO thin films.

The high resistivities of the low-pressure sputtered films originated from their dense, fibrous structures and their low carrier concentrations. In order to overcome these high resistivities, we designed complementary stacked structures consisting of continuous two-step deposited ITO films. To achieve this, the initial layer was deposited by ULPS and the final layer was deposited using a pressure of $6.7 \times 10^{-1} \text{ Pa}$. Using this method, we achieved an extremely smooth surface roughness of approximately 0.8 nm with a low resistivity of $3.7 \times 10^{-4} \Omega \text{ cm}$. The columns of the second layer (about 130 nm in diameter) in the continuous TSF were about 2.5 times wider than those (about 50 nm in diameter) of the films

sputtered at $6.7 \times 10^{-1} \text{ Pa}$. This advantage makes our ULPS method useful for the production of high-quality ITO thin films.

Seoul National University assisted in meeting the publication costs of this article.

References

- S. Ray, R. Banerjee, N. Basu, A. K. Batabyal, and A. K. Barua, *J. Appl. Phys.*, **54**, 3497 (1983).
- S. Y. Kim, K. Kim, Y. Tak, and J. Lee, *J. Appl. Phys.*, **95**, 2560 (2004).
- J. C. C. Fan, F. J. Bachner, and G. H. Foley, *Appl. Phys. Lett.*, **31**, 773 (1997).
- M. Higuchi, M. Sawada, and Y. Kuronuma, *J. Electrochem. Soc.*, **140**, 1773 (1993).
- C. Guillen and J. Herrero, *J. Appl. Phys.*, **101**, 073514 (2007).
- A. K. Saxena, S. P. Singh, R. Thangaraj, and O. P. Agnihotri, *Thin Solid Films*, **117**, 95 (1984).
- M. Ando, E. Nishimura, K.-I. Onisawa, and T. Minemura, *J. Appl. Phys.*, **93**, 1032 (2002).
- R. X. Wang, C. D. Beling, S. Fung, A. Djuric, C. C. Ling, and S. Li, *J. Appl. Phys.*, **97**, 033504 (2005).
- F. O. Adurodiwa, L. Semple, and R. Bruning, *Thin Solid Films*, **492**, 153 (2005).
- D. Kim, *Vacuum*, **81**, 279 (2006).
- S. Iwatsubo, *Vacuum*, **80**, 708 (2006).
- G. Choi, Y. Seo, K. Lee, and W. Lee, *J. Vac. Sci. Technol. A*, **25**, 999 (2007).
- K. B. Kim, Y. H. Tak, Y. S. Han, K. H. Baik, M. H. Yoon, and M. H. Lee, *Jpn. J. Appl. Phys., Part 2*, **42**, L438 (2003).
- L. S. Liao, J. He, X. Zhou, M. Lu, Z. H. Xiong, Z. B. Deng, X. Y. Hou, and S. T. Lee, *J. Appl. Phys.*, **88**, 2386 (2000).
- C. Liu, T. Matsutani, T. Asanuma, K. Murai, M. Kiuchi, and R. S. Robinson, *J. Appl. Phys.*, **93**, 2262 (2003).
- M. Jung and H. Choi, *J. Electrochem. Soc.*, **155**, H334 (2008).
- T. J. Vink, W. Walrave, J. L. C. Daams, P. C. Baarslag, and J. E. A. M. Meerakker, *Thin Solid Films*, **266**, 145 (1995).
- J. E. A. M. Meerakker, P. C. Baarslag, W. Walrave, T. J. Vink, and J. L. C. Daams, *Thin Solid Films*, **266**, 152 (1995).
- M. Hoheisel, A. Mitwalsky, and C. Mrotzek, *Phys. Status Solidi A*, **123**, 461 (1991).
- D. G. Neerinck and T. J. Vink, *Thin Solid Films*, **278**, 12 (1996).
- J. A. Thornton and D. W. Hoffman, *Thin Solid Films*, **171**, 5 (1989).
- L. I. Maissel and R. Glang, *Handbook of Thin Film Technology*, pp. 3–21, McGraw-Hill, New York (1970).
- K. Meyer, I. K. Schuller, and C. M. Falco, *J. Appl. Phys.*, **52**, 5803 (1981).
- R. S. Robinson, *J. Vac. Sci. Technol.*, **16**, 185 (1979).
- H. F. Winters and E. Kay, *J. Appl. Phys.*, **38**, 3928 (1967).
- H. Han, J. W. Mayer, and T. L. Alford, *J. Appl. Phys.*, **100**, 083715 (2006).
- S.-I. Jun, T. E. McKnight, M. L. Simpson, and P. D. Rack, *Thin Solid Films*, **476**, 59 (2005).
- H. Kim, C. M. Gilmore, A. Pique, J. S. Horwitz, H. Murata, Z. H. Kafai, and D. B. Chrisey, *J. Appl. Phys.*, **86**, 6451 (1999).
- E. Burstein, *Phys. Rev.*, **93**, 632 (1954).
- H. L. Hartnagel, A. L. Dawar, A. K. Jain, and C. Jagadish, *Semiconducting Transparent Thin Films*, p. 244, Institute of Physics Publishing, Bristol (1995).
- C. Yang, S. Lee, T. Lin, and S. Chen, *Thin Solid Films*, **516**, 1984 (2008).
- Y. Sato, R. Tokumaru, E. Nishimura, P. K. Song, and Y. Shigesato, *J. Vac. Sci. Technol. A*, **23**, 1167 (2005).
- M. Buchanan, J. B. Webb, and D. F. Williams, *Appl. Phys. Lett.*, **37**, 213 (1980).
- W. G. Haines and R. H. Bube, *J. Appl. Phys.*, **49**, 304 (1978).
- H. Morikawa and M. Fujita, *Thin Solid Films*, **339**, 309 (1999).
- Y. Ohhata, F. Shinoki, and S. Yoshida, *Thin Solid Films*, **59**, 225 (1979).
- S. Ishibashi, Y. Higuchi, Y. Ota, and K. Nakamura, *J. Vac. Sci. Technol. A*, **A8**, 1399 (1990).
- G. Haake, *J. Appl. Phys.*, **47**, 4086 (1976).